

# Coherent storage and phase modulation of single hard x-ray photons using nuclear excitons

Wen-Te Liao,<sup>\*</sup> Adriana Pálffy,<sup>†</sup> and Christoph H. Keitel

*Max-Planck-Institut für Kernphysik, Saupfercheckweg 1, D-69117 Heidelberg, Germany*

(Dated: June 4, 2019)

## Abstract

Phase-sensitive photon storage of hard x-rays in resonant scattering of light off nuclei is investigated theoretically. We show that by switching off and on again the magnetic field in the nuclear sample, phase-sensitive storage of keV-photon pulses can be achieved. Corresponding  $\pi$  phase modulation of the stored photon is possible if the retrieving magnetic field is rotated by  $180^\circ$ . As phase control tests we put forward a two-target setup that allows for the formation of a magnetically induced nuclear exciton echo and presents in itself another alternative for single-photon storage. These control techniques for a single photon in the 10 keV range may provide the potential of substantially shrinking future photonic devices.

PACS numbers: 78.70.Ck, 42.50.Md, 42.50.Nn, 76.80.+y

Keywords: x-ray quantum optics, x-ray free electron laser, interference effects, nuclear forward scattering

---

<sup>\*</sup>Electronic address: Wen-Te.Liao@mpi-hd.mpg.de

<sup>†</sup>Electronic address: Palfy@mpi-hd.mpg.de

The development of modern x-ray sources has come to extend quantum optics to the x-ray region in exciting applications such as controlling the x-ray refractive index in atomic and nuclear systems [1, 2], the Autler-Townes effect [3] and electromagnetically induced transparency (EIT) for x-rays [4, 5], or entanglement with keV photons via spontaneous parametric down-conversion [6]. With the shift to higher frequencies, also new physical systems come into play, e.g., nuclei with low-lying collective states naturally arise as candidates for x-ray quantum optics studies. The advent of the x-ray free electron laser (XFEL) [7, 8] has opened the possibility to investigate nuclear quantum optics [9] and nuclear coherent population transfer [10]. Further coherent control tools based on nuclear cooperative effects [11–14] are known also from nuclear forward scattering (NFS) experiments with third-generation light sources. A key example in this direction is how manipulation of the hyperfine magnetic field in NFS systems provides means to control single x-ray photons, in storage of nuclear excitation energy [15] and generation of keV single-photon entanglement [16].

Coherent control at high frequencies may develop the traditional x-ray imaging towards better precision and non-destructive measurements performed with single or few photons. Furthermore, from a practical point of view, forwarding optics and quantum information to shorter wavelengths in the x-ray region has the potential of shrinking computing elements in future photonic devices such as the quantum photonic circuit [17]. The small diffraction limit of x-rays is guaranteed to prevent any obstacles in the fabrication technology towards most compact devices [18]. However, such tasks require mastery of x-ray optics and powerful control tools of single-photon wave packet amplitude, frequency, polarization and phase [19]. The development of x-ray optics elements had made already significant progress with the realization of x-ray diamond mirrors [20–22] and cavities [23], hard x-ray waveguides [24, 25] and the Fabry-Pérot resonator [26–28]. Efficient phase-sensitive photon storage for photon delay lines and x-ray phase modulation, preferably even for single-photon wave packets, are next milestones to be reached.

Here, we present two important control tools for hard x-rays photons using resonant scattering of light off nuclei in a NFS setup. The delocalized nature of the nuclear excitation produced by coherent XFEL or synchrotron radiation (SR) light, i.e., the formation of a nuclear exciton, opens the possibility to control the coherent decay and therefore emission of scattered light. Making use of this feature, we first put forward how to store a single hard x-ray photon for time intervals of 10-100 ns by turning off the hyperfine magnetic field in a NFS system. The stored single photon can be released by turning on the magnetic field. We emphasize that our scheme conserves not only the excitation energy, as already demonstrated in Ref. [15], but also the photonic polarization

and phase beyond the ps time range. Next, we show how to modulate the stored photon with a phase shift of  $\pi$  by using a releasing hyperfine magnetic field oriented in the opposite direction to the initial one. For the measurement of this  $\pi$ -phase shift of the retrieved photon, we refer to the echo technique using two nuclear targets [29–31] and demonstrate for the first time a magnetically induced nuclear exciton echo without any mechanical vibration of the targets. This echo two-sample setup can also be used for polarization-sensitive photon storage involving a mere rotation of the hyperfine magnetic field by  $180^\circ$ . The experimental feasibility of our storage schemes is discussed.

The typical NFS setup is presented in Fig. 1(a). The enriched  $^{57}\text{Fe}$  target is depicted by the green cuboid. The incident x-ray pulse can be either SR or coherent XFEL light. SR typically produces at most one excited nucleus per pulse, thus providing a reliable single-excitation and single released photon scenario. The disadvantage here is that the initial photonic phase is undefined. On the other hand, coherent x-ray light from seeded or oscillator XFEL [32–34] with a well-defined photonic phase can be used at low intensities such as to keep the excitation rate below one nucleus per pulse in the sample if single photons are desirable. An externally applied magnetic field  $\mathbf{B}$  in the  $z$  direction induces the nuclear hyperfine splitting of the ground and excited  $^{57}\text{Fe}$  nuclear states illustrated in Fig. 1(b). The hyperfine splitting causes the quantum beat [35, 36] typically visible in NFS time spectra. An x-ray pulse with meV or sub-meV bandwidth tuned on the 14.413 keV nuclear transition energy scatters off the nuclear target parallel to the  $y$  direction. Depending on the pulse polarization, different hyperfine transitions will be driven. In Fig. 1(a), the linearly polarized x-ray field drives the  $\Delta m = m_e - m_g = 0$  transitions indicated by arrows in Fig. 1(b).

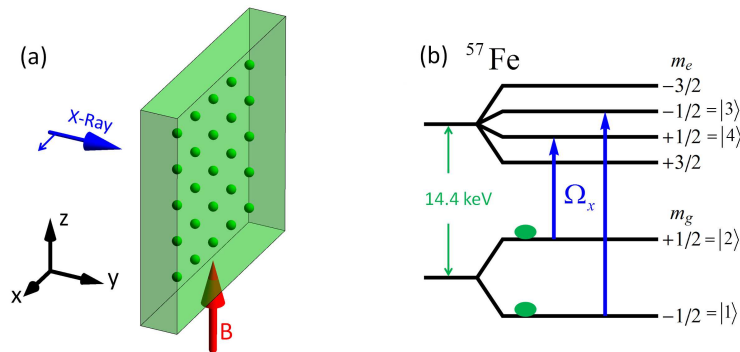


FIG. 1: (a) Nuclear forward scattering setup. The blue arrow depicts the linear polarized x-ray pulse propagating in  $y$  direction and  $\mathbf{B}$  is the external magnetic field initially parallel to the  $z$ -axis. (b) Hyperfine level structure of  $^{57}\text{Fe}$ . The blue solid arrows denote the  $\Delta m = m_e - m_g = 0$  transitions driven by the x-ray pulse which is linearly polarized in the  $x$  direction.

The notation  $m_e$  and  $m_g$  is used for the projections of the nuclear spin on the quantization axis.

We consider the  $M1$  transition of  $^{57}\text{Fe}$  from the ground state to the first excited state at 14.413 keV, namely the two transitions with  $\Delta m = 0$  among the six-level system denoted in Fig. 1(b). The dynamics of the density matrix  $\hat{\rho}$  is governed by the Maxwell-Bloch equations [37–40]:

$$\begin{aligned} \partial_t \hat{\rho} &= \frac{1}{i\hbar} [\hat{H}, \hat{\rho}] + \hat{\rho}_s, \\ \frac{1}{c} \partial_t \Omega_x + \partial_y \Omega_x &= i\eta (a_{31}\rho_{31} + a_{42}\rho_{42}), \end{aligned} \quad (1)$$

with the interaction Hamiltonian

$$\hat{H} = -\frac{\hbar}{2} \begin{pmatrix} 2\Delta_g & 0 & a_{13}\Omega_x^* & 0 \\ 0 & -2\Delta_g & 0 & a_{24}\Omega_x^* \\ a_{31}\Omega_x & 0 & -2(\Delta + \Delta_e) & 0 \\ 0 & a_{42}\Omega_x & 0 & -2(\Delta - \Delta_e) \end{pmatrix}.$$

In the equations above  $\Delta$  is the x-ray detuning to the 14.4 keV transition assumed to be zero and  $\Delta_{g(e)}$  denotes the Zeeman energy splitting of the nuclear ground (excited) state proportional to the magnetic field  $\mathbf{B}$ . In Eq. (1),  $\rho_{eg} = A_e A_g^*$  for  $\{e, g\} \in \{1, 2, 3, 4\}$  are the density matrix elements of  $\hat{\rho}$  for the nuclear wave function  $|\psi\rangle = A_1|1\rangle + A_2|2\rangle + A_3|3\rangle + A_4|4\rangle$ , where the ket vectors are the eigenvectors depicted in Fig. 1(b). Furthermore,  $a_{eg} = a_{ge} = \sqrt{2/3}$  are the corresponding Clebsch-Gordan coefficients [35, 40] for the  $\Delta m = 0$  transitions and  $\hat{\rho}_s$  describes the spontaneous decay [39]. The parameter  $\eta$  is defined as  $\eta = \frac{6\Gamma}{L}\alpha$ , where  $\Gamma = 1/141.1$  GHz is the spontaneous decay rate of excited states,  $\alpha$  represents the effective resonant thickness [35, 37, 38] and  $L = 10$

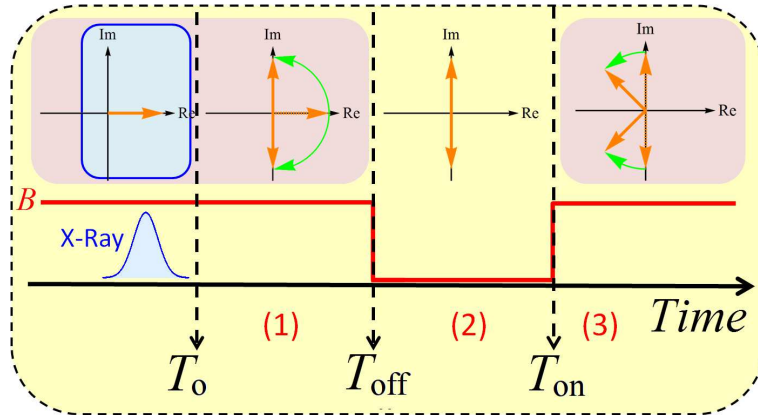


FIG. 2: The time dependence of the hyperfine magnetic field  $\mathbf{B}$  (red line) and the corresponding dynamics of the nuclear currents (orange arrows). The dynamics will be surveyed in three temporal domains: (1)  $T_0 < t < T_{\text{off}}$ ; (2)  $T_{\text{off}} < t < T_{\text{on}}$ ; (3)  $T_{\text{on}} < t$ .

$\mu\text{m}$  the thickness of the target, respectively. Further notations are  $\Omega_x$  for the Rabi frequency which is proportional to the electric field  $\vec{E}_x$  of the x-ray pulse [39, 40] and  $c$  the speed of light.

Fig. 2 illustrates the time evolution of our photon storage scheme. The external magnetic field  $\mathbf{B}$ , depicted by the red line, is present before the x-ray pulse impinges on the target at  $T_o$ . At  $T_{\text{off}}$  the  $\mathbf{B}$  field is turned off and later turned back on at  $T_{\text{on}}$ . Additionally, the orange arrows in Fig. 2 demonstrate the time evolution of the nuclear transition current matrix elements as defined in Ref. [15]. In our treatment, this is equivalent with investigating the coherence terms  $i\rho_{42}$  and

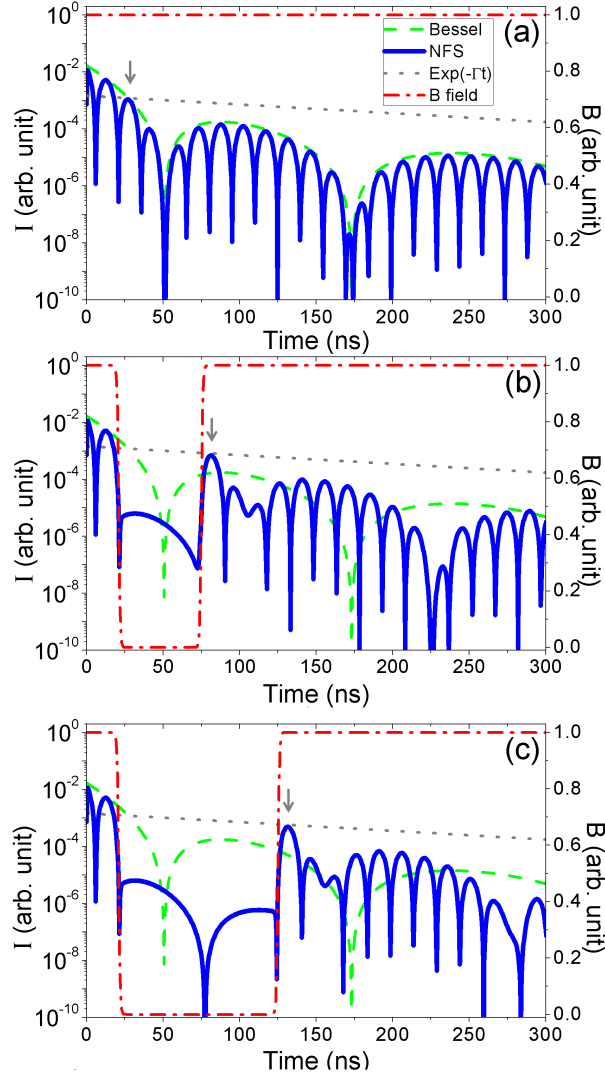


FIG. 3: (a) The unperturbed NFS time spectrum with  $\Delta_B = 15\Gamma$  and  $\alpha = 10$ . Blue solid lines are the intensities of the NFS signal, red dashed dotted lines denote qualitatively the applied magnetic field  $\mathbf{B}$ , the gray dotted lines are proportional to  $e^{-\Gamma t}$  and the green dashed lines are proportional to  $\left(\frac{\alpha}{\sqrt{\alpha\Gamma t}} J_1\left[2\sqrt{\alpha\Gamma t}\right]\right)^2 e^{-\Gamma t}$  [36, 37]. In (b-c), the hyperfine magnetic field is turned off at  $t = 21$  ns, and turned back on at (b)  $t = 75$  ns and (c)  $t = 125$  ns.

$i\rho_{31}$  [37, 38].

Initially, the ensemble of  $^{57}\text{Fe}$  nuclei is excited by the x-ray pulse at  $T_o$ . Subsequently, the purely real currents are abruptly built. In the time interval (1), the two currents start to rotate in opposite directions on the complex plane with the factor of  $e^{\pm i\Delta_B t}$  caused by the magnetic field until  $t = T_{\text{off}}$  when  $\mathbf{B}$  is turned off. The corresponding phase gain is  $\pm \Delta_B \tau$ . Here and in the following we have used for simplicity the notations  $\Delta_B = \Delta_g + \Delta_e$  and  $\tau = T_{\text{off}} - T_o$ . Within the time interval (2), the quantum beat (arising from the interference between the two  $\Delta m = 0$  transitions) is frozen with the factor of  $e^{\pm i\Delta_B \tau}$  since the hyperfine field has vanished, and only the dynamical beat [11, 35, 37] due to interference between multiple scattering processes in the sample persists. During the time interval (3), the presence of the magnetic field makes the quantum beat emerge again.

We numerically solve Eq. (1) with  $\alpha = 10$  and  $\Delta_B = 15\Gamma$ , and present our photon storage results in Figs. 3 and 4. The NFS signal intensities  $|\vec{E}_x(t, L)|^2$  are compared with the spontaneous decay curves  $e^{-\Gamma t}$  and the pure dynamical beat (for the case of no hyperfine splitting)  $\left(\frac{\alpha}{\sqrt{\alpha\Gamma t}} J_1 \left[2\sqrt{\alpha\Gamma t}\right]\right)^2 e^{-\Gamma t}$  [36, 37], where  $J_1$  is the Bessel function of first kind. Fig. 3(a) shows the unperturbed NFS time spectrum where both quantum beat and dynamical beat are observed. In Fig. 3(b) and (c) we demonstrate photon storage by turning off the magnetic field at  $t = 21$  ns (corresponding to a quantum beat minimum,  $\Delta_B \tau = \pm N\frac{\pi}{2}$  with  $N$  odd). Both nuclear currents corresponding to the  $\Delta m = 0$  transitions are frozen on the imaginary axis (see Fig. 2) and undergo destructive interference. In this case the intensity of the emitted radiation is significantly suppressed, being three orders of magnitude smaller compared to the unperturbed spectrum. Later on, by turning the hyperfine magnetic field on again at (b)  $t = 75$  ns and (c)  $t = 125$  ns, the unsuppressed photon signal is observed again within the time interval (3). Fig. 3 also shows that the stored nuclear excitation energy experiences spontaneous decay during the storage time [15].

The electric field envelopes of the scattered photon are presented in Fig. 4. In Fig. 4(a), the magnetic field before  $T_{\text{off}} = 80.5$  ns and that after  $T_{\text{on}} = 175$  ns are the same and the phase before storage and after retrieving is continuous in this case. If, however, the retrieving magnetic field is applied in opposite direction as shown in Fig. 4(b), the phase of the released photon will be modulated with a shift of  $\pi$ . This is caused by the effect of reversed time related with the change of sign of the hyperfine magnetic field [41, 42], i.e., all the nuclear currents evolve backwards in time. Our density matrix calculations have been double-checked by the comparison with results from the iterative solution of the wave equations originally proposed by Shvyd'ko [15]. The agreement is complete for both electric field envelope and scattered light intensity, proving the equivalence

of the two methods.

The most significant advantage of our scheme is the conservation of the photonic polarization and phase. Storage of nuclear excitation energy by magnetic field rotations in NFS experiments with SR was presented in Ref. [15]. This pioneering work has opened the avenue of coherent control applications with nuclei using magnetic switching. However, the scheme in Ref. [15] is not phase-sensitive. Since the magnetic Hamiltonian is not zero during the storage, both the polarization [43] and the phase of the particular polarization components cannot be stored and the properties of the released photon depend on the switching instants. While for experiments with incoherent SR phase information can be disregarded, with the advent of coherent XFEL sources and x-ray quantum optics experiments, phase storage and modulation becomes crucial for many applications. So far, coherent trapping of hard x-rays in crystal cavities provides photon storage for time intervals in the ps range [23]. Our scheme provides robust phase and polarization storage of the x-ray photon on the 10-100 ns scale determined by the nuclear lifetime.

In order to implement our phase-sensitive storage scheme experimentally, a material with no intrinsic nuclear Zeeman splitting like stainless steel  $\text{Fe}_{55}\text{Cr}_{25}\text{Ni}_{20}$  [29, 30] is required. The remaining challenge is to turn off and on the external magnetic fields of few Tesla on the ns time scale. According to our calculations for the case of Fig. 3, the raising time of the  $\mathbf{B}$  field should be shorter than 50 ns (the raising time was considered 4 ns for all presented cases). This could be achieved by using small single- or few-turn coils and a moderate pulse current of approx. 15 kA

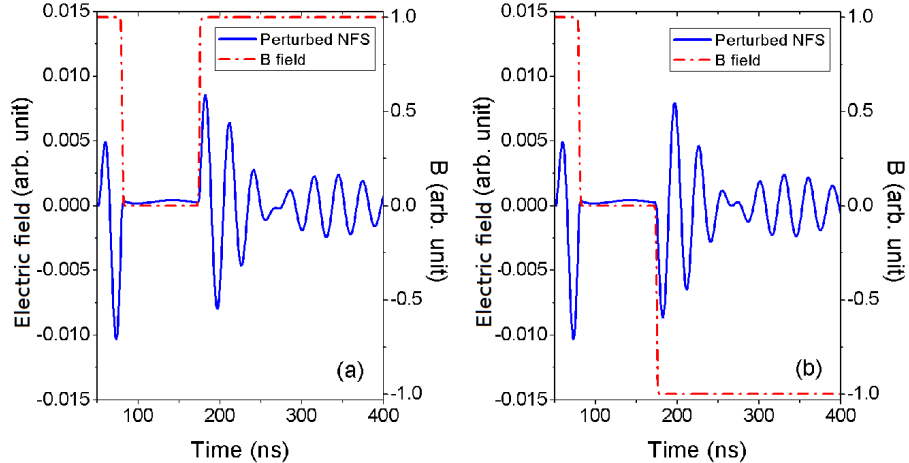


FIG. 4: Phase modulation of retrieved x-ray via reversing the applied magnetic field  $\mathbf{B}$ . Blue solid lines are the electric field of NFS signal, red dashed lines denote the applied magnetic fields  $\mathbf{B}$ . The  $\mathbf{B}$  field is turned off at  $T_{\text{off}} = 80.5$  ns and then switched on at  $T_{\text{on}} = 175$  ns, such that (a)  $\mathbf{B}(t < T_{\text{off}}) = \mathbf{B}(t > T_{\text{on}})$  and (b)  $\mathbf{B}(t < T_{\text{off}}) = -\mathbf{B}(t > T_{\text{on}})$ . Comparing with (a), the phase of retrieved x-ray is modulated by  $\pi$  in (b).

from low-inductive high-voltage “snapper” capacitors [44]. Another mechanical solution, e.g., the lighthouse setup [45] could be used to bring the excited target out and in a region with confined static  $\mathbf{B}$  field. We estimate that a rotor with rotational frequencies of up to 70 kHz and a diameter of few mm [13] is fast enough to rotate the sample out a depth of few  $\mu\text{m}$  in a few tens of ns.

Let us now turn to the measurement of the  $\pi$  phase shift. A typical x-ray optics setup would require to let the  $\pi$ -modulated photon interfere with a part of the original pulse on a triple Laue interferometer [46, 47]. We adopt here another approach, namely, the simple and elegant photon echo solution used in NFS experiments with SR to allow the scattered photon to interfere with itself in a two-target setup. Mechanical x-ray phase modulation was demonstrated in this manner in studies of coherent transient effects [48], gamma echos [49] and nuclear exciton echos [29–31]. Our two-targets setup is presented in Fig. 5. A dynamical magnetic field  $\mathbf{B}_1(t)$  is applied to target 1, and a static  $\mathbf{B}_2$  is applied to target 2. The target response is determined by  $R(\alpha, \Delta_B, t) = \delta(t) - W(\alpha, \Delta_B, t)$  and  $W(\alpha, \Delta_B, t) = \frac{\alpha}{\sqrt{\alpha\Gamma t}} J_1\left(2\sqrt{\alpha\Gamma t}\right) e^{-\frac{\Gamma}{2}t + i\Delta_B t}$  [49], and the forward-scattered x-ray field is then given by  $E^{(1)}(t) = \int_0^t R(\alpha, \Delta_B, t - \tau) E^{(0)}(\tau) d\tau$  [31]. Using  $E^{(0)}(t) = \delta(t)$  as x-ray input, the resulting electric field registered by the detector is the real part of

$$E^{(2)}(t) = \delta(t) - W(\alpha_1, \Delta_{B1}, t) - W(\alpha_2, \Delta_{B2}, t) + \int_0^t W(\alpha_2, \Delta_{B2}, t - \tau) W(\alpha_1, \Delta_{B1}, \tau) d\tau. \quad (2)$$

This depicts the interference of four possible coherent scattering channels [31]: (1)  $\delta(t)$ , no scattering; (2)  $-W(\alpha_1, \Delta_{B1}, t)$ , the photon is scattered by target 1 only; (3)  $-W(\alpha_2, \Delta_{B2}, t)$ , the photon is scattered by target 2 only; (4) the mutual integral, the photon is first scattered by target 1 and then by target 2. It is easy to see that channel (2) and (3) will cancel each other out when the

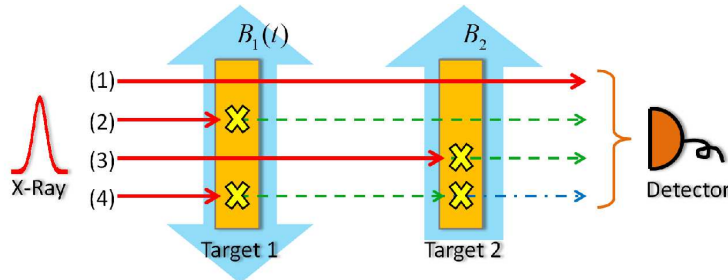


FIG. 5: The setup of magnetically induced nuclear exciton echo with two targets. The orange rectangles depict the targets, and the red pulse the input x-ray. Yellow crosses illustrate the formation of the nuclear exciton. The light blue up-down thick arrows show the applied magnetic fields: the dynamical  $\mathbf{B}_1(t)$  is applied to target 1, whereas the static  $\mathbf{B}_2$  is applied to target 2. (1)(2)(3)(4) are four possible coherent scattering channels (see text for details).

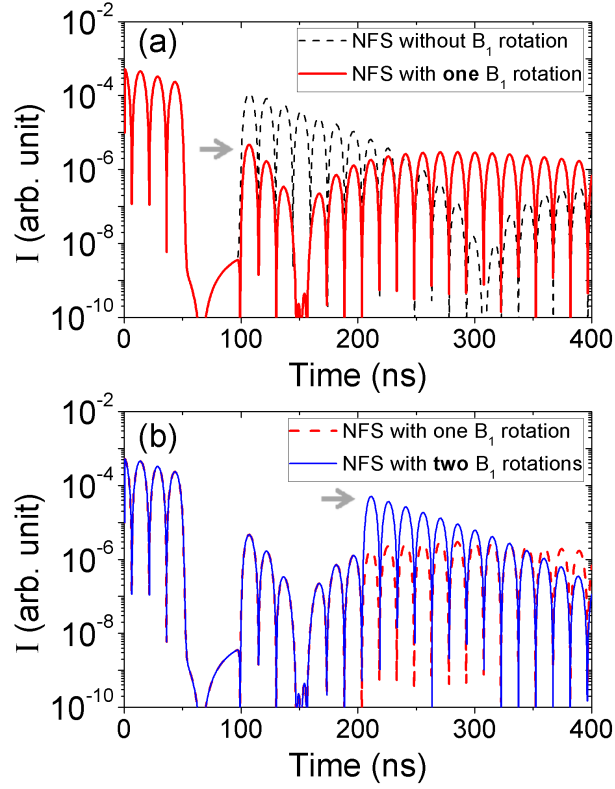


FIG. 6: Magnetically induced nuclear exciton echo using  $\alpha_1 = \alpha_2 = 1$  and  $|\Delta_{B_1}| = \Delta_{B_2} = 15\Gamma$ . The magnetic field  $\mathbf{B}_1(t)$  is turned off at  $T_{\text{off}} = 51$  ns and on at  $T_{\text{on}} = 100$  ns. The black dashed line denotes the case of  $\mathbf{B}_1(t > T_{\text{on}}) = \mathbf{B}_1(t < T_{\text{off}})$ , the red solid line and red dotted line illustrate the case of  $\mathbf{B}_1(t > T_{\text{on}}) = -\mathbf{B}_1(t < T_{\text{off}})$ . The blue solid line in (b) depicts the magnetically induced nuclear exciton echo with  $\mathbf{B}_1(204.3\text{ns} > t > T_{\text{on}}) = -\mathbf{B}_1(t > 204.3\text{ns}) = -\mathbf{B}_1(t < T_{\text{off}})$ , i.e.,  $\mathbf{B}_1(t)$  is rotated back at  $t = 204.3$  ns. The gray arrows mark the instant when the magnetic field is rotated: (a) the first time, (b) the second time.

effective thicknesses of the two targets are equal  $\alpha_1 = \alpha_2$  and  $\mathbf{B}_1(t > T_{\text{on}}) = -\mathbf{B}_2$ , i.e.,  $\mathbf{B}_1(t)$  is reversed at  $t = T_{\text{on}}$ . Hence one can observe when the NFS signal is significantly suppressed once the effective  $\pi$  phase shift is magnetically modulated in target 1.

Fig. 6 shows our numerical results with  $\alpha_1 = \alpha_2 = 1$ ,  $|\Delta_{B_1}| = \Delta_{B_2} = 15\Gamma$ ,  $T_{\text{off}} = 51$  ns and  $T_{\text{on}} = 100$  ns. The presence of two target results in the faster coherent decay (red dashed line) that proceeds with effective resonant depth of  $\alpha = 2$ , i.e., double the thickness of each target [29]. The magnetic field in target 1 is switched off at  $T_{\text{off}} = 51$  ns and back on at  $T_{\text{on}} = 100$  ns. For continuous phase, the intensity of the scattered field does not change. If, however, the phase of the retrieved field is  $\pi$ -modulated by turning on the opposite magnetic field  $-\mathbf{B}_1$ , the detected signal is significantly suppressed. The difference between the two retrieving scenarios is presented in Fig. 6(a). Similarly to our storage scheme for one target, it is destructive interference between

two scattering channels that leads to this effect. To confirm that the destructive interference of scattering channel (2) and (3) causes this suppression, we further check the effect of a magnetic field rotation back at a node value  $E^{(1)}(t > 100 \text{ ns}) = 0$ . Then the NFS after the second rotation of  $\mathbf{B}_1$  should be enhanced like an echo. This magnetically induced nuclear exciton echo is visible in Fig. 6(b) when we rotate the magnetic field  $\mathbf{B}_1(t)$  back at  $t = 204.3 \text{ ns}$ .

It becomes apparent that the magnetically induced nuclear exciton echo itself also provides another convenient solution for polarization-sensitive photon storage: inverse magnetic fields in target 1 and 2 lead to a significant suppression of the scattered x-ray light. A sequence of two  $180^\circ$  rotations of the magnetic field direction in target 1 at the quantum beat minima can therefore lead to storage and retrieval of the x-ray photon  $\pi$  phase-modulated. This can be experimentally achieved in antiferromagnets as  $^{57}\text{FeBO}_3$  with strong intrinsic hyperfine magnetic fields that can be rotated with the help of a weak 10 G external field [15]. Fast  $180^\circ$  magnetic field rotations in such materials have been successfully performed [41]. This specific case of magnetic switching in a two-target setup preserves the photon polarization and can modulate the photonic phase but it is less robust compared to our scheme since both efficiency of the storage and the phase of the released photon depend on the rotation moment. Nevertheless, the magnetically induced nuclear exciton echo might provide an additional experimentally accessible setup to investigate mechanical-free x-ray storage and phase modulation in the near future.

In conclusion, we have demonstrated phase-sensitive storage and  $\pi$  phase modulation for single hard x-ray photons. As a step forward towards feasible control schemes in x-ray nuclear quantum optics, we believe our results will help extend Moore's law [18] to the future photonic devices.

We would like to thank R. Röhlsberger for fruitful discussions and T. Herrmannsdörfer for his advice on the generation of strong magnetic fields.

- 
- [1] C. Buth and R. Santra. *Phys. Rev. A*, 78, 043409 (2008).
  - [2] R. Coussement et al. *Phys. Rev. Lett.*, 89, 107601 (2002).
  - [3] T. E. Glover et al. *Nature Phys.*, 6, 69 (2009).
  - [4] C. Buth, R. Santra, and L. Young. *Phys. Rev. Lett.*, 98, 253001 (2007).
  - [5] R. Röhlsberger et al. *Nature*, 482, 199 (2012).
  - [6] S. Schwartz and S. E. Harris. *Phys. Rev. Lett.*, 106, 080501 (2011).
  - [7] J. Arthur et al. *Linac Coherent Light Source (LCLS). Conceptual Design Report*. SLAC, Stanford,

2002.

- [8] Massimo Altarelli et al. *XFEL: The European X-Ray Free-Electron Laser. Technical Design Report*. DESY, Hamburg, 2006.
- [9] T. J. Bürvenich, J. Evers, and C. H. Keitel. *Phys. Rev. Lett.*, 96, 142501 (2006).
- [10] W. T. Liao, A. Pálffy, and C. H. Keitel. *Phys. Lett. B*, 705, 134 (2011).
- [11] U. Van Bürck. *Hyperfine Interact.*, 123, 483 (1999).
- [12] Yu. V. Shvyd'ko. *Hyperfine Interact.*, 125, 173 (2000).
- [13] R. Röhlsberger. *Nuclear Condensed Matter Physics With Synchrotron Radiation: Basic Principles, Methodology and Applications*. Springer-Verlag, 2004.
- [14] R. Röhlsberger et al. *Science*, 328, 1248 (2010).
- [15] Yu. V. Shvyd'ko et al. *Phys. Rev. Lett.*, 77, 3232 (1996).
- [16] A. Pálffy, C. H. Keitel, and J. Evers. *Phys. Rev. Lett.*, 103, 017401 (2009).
- [17] A. Politi et al. *Science*, 320, 646 (2008).
- [18] G. E. Moore. *Proc. IEEE*, 86, 82 (1998).
- [19] H. P. Specht, J. Bochmann, M. Mücke, B. Weber, E. Figueroa, D. L. Moehring, and G. Rempe. *Nature Photon.*, 3, 469 (2009).
- [20] Yu. Shvyd'ko. *X-Ray Optics: High-Energy-Resolution Applications*. Springer-Verlag, 2004.
- [21] Yu. Shvyd'ko, S. Stoupin, A. Cunsolo, A. H. Said, and X. Huang. *Nature Phys.*, 6, 196 (2010).
- [22] Yu. Shvyd'ko, S. Stoupin, V. Blank, and S. Terentyev. *Nature Photon.*, 5, 539 (2011).
- [23] S.-Y. Chen, H.-H. Wu, Y.-Y. Chang, Y.-R. Lee, W.-H. Sun, S.-L. Chang, Yu. P. Stetsko, M.-T. Tang, M. Yabashi, and T. Ishikawa. *Appl. Phys. Lett.*, 93:141105, 2008.
- [24] F. Pfeiffer, C. David, M. Burghammer, C. Riekell, and T. Salditt. *Science*, 297, 230 (2002).
- [25] A. Jarre, C. Fuhse, C. Ollinger, J. Seeger, R. Tucoulou, and T. Salditt. *Phys. Rev. Lett.*, 94:074801, 2005.
- [26] K.-D. Liss, R. Hock, M. Gomm, B. Waibel, A. Magerl, M. Krisch, and R. Tucoulou. *Nature*, 404, 371 (2000).
- [27] Yu. V. Shvyd'ko, M. Lerche, H.-C. Wille, E. Gerdau, M. Lucht, H. D. Rüter, E. E. Alp, and R. Khachatryan. *Phys. Rev. Lett.*, 90:013904, 2003.
- [28] S.-L. Chang, Yu. P. Stetsko, M.-T. Tang, Y.-R. Lee, W.-H. Sun, M. Yabashi, and T. Ishikawa. *Phys. Rev. Lett.*, 94:174801, 2005.
- [29] G. V. Smirnov et al. *Phys. Rev. Lett.*, 77, 183 (1996).
- [30] H. Jex et al. *Europhys. Lett.*, 40, 317 (1997).

- [31] G. V. Smirnov et al. *Phys. Rev. A*, 71, 023804 (2005).
- [32] J. Feldhaus, E. L. Saldin, J. R. Schneider, E. A. Schneidmiller, and M. V. Yurkov. *Opt. Commun.*, 140:341, 1997.
- [33] E. L. Saldin, E. A. Schneidmiller, Yu. V. Shvyd'ko, and M. V. Yurkov. *Nucl. Instrum. Methods A*, 475:357, 2001.
- [34] Kwang-Je Kim, Yuri Shvyd'ko, and Sven Reiche. *Phys. Rev. Lett.*, 100(24):244802, Jun 2008.
- [35] Yu. V. Shvyd'ko et al. *Phys. Rev. B*, 57, 3552 (1998).
- [36] Yu. V. Shvyd'ko and U. Van Bürck. *Hyperfine Interact.*, 123, 511 (1999).
- [37] M. D. Crisp. *Phys. Rev. A*, 1, 1604 (1970).
- [38] Yu. V. Shvyd'ko. *Phys. Rev. B*, 59, 9132 (1999).
- [39] M. O. Scully and M. S. Zubairy. *Quantum Optics*. Cambridge University Press, 2006.
- [40] A. Pálffy, J. Evers, and C. H. Keitel. *Phys. Rev. C*, 77, 044602 (2008).
- [41] Yu. V. Shvyd'ko. *Hyperfine Interact.*, 90, 287 (1994).
- [42] Yu. V. Shvyd'ko et al. *Phys. Rev. B*, 52, R711 (1995).
- [43] A. Pálffy and J. Evers. *J. Mod. Opt.*, 57, 1993 (2010).
- [44] N. Miura, T. Osada, and S. Takeyama. *J. Low Temp. Phys.*, 133(1):139–158, 2003.
- [45] R. Röhlsberger et al. *Phys. Rev. Lett.*, 84, 1007 (2000).
- [46] Y. Hasegawa, Y. Yoda, K. Izumi, T. Ishikawa, S. Kikuta, X. W. Zhang, and M. Ando. *Phys. Rev. Lett.*, 75:2216–2219, 1995.
- [47] Y. Hasegawa and S. Kikuta. *Hyperfine Interact.*, 123-124:721, 1999.
- [48] P. Heliö et al. *Phys. Rev. Lett.*, 49, 1209 (1982).
- [49] P. Heliö et al. *Phys. Rev. Lett.*, 66, 2037 (1991).